Journal of Asian Earth Sciences 98 (2015) 272–284

Contents lists available at ScienceDirect

Journal of Asian Earth Sciences

journal homepage: www.elsevier.com/locate/jseaes

Geology, isotope geochemistry and geochronology of the Jinshachang carbonate-hosted Pb–Zn deposit, southwest China

Jia-Xi Zhou [a,b,*], Jun-Hao Bai [c], Zhi-Long Huang [a], Dan Zhu [a], Zai-Fei Yan [a], Zhi-Cheng Lv [b]

[a] State Key Laboratory of Ore Deposit Geochemistry, Institute of Geochemistry, Chinese Academy of Sciences, Guiyang 550002, China
[b] Development and Research Center, China Geological Survey, Beijing 100037, China
[c] Henan Academy of Land and Resources, Zhengzhou 450053, China

ARTICLE INFO

Article history:
Received 28 April 2014
Received in revised form 13 November 2014
Accepted 27 November 2014
Available online 3 December 2014

Keywords:
H–O–S and Pb isotopes
Sphalerite Rb–Sr dating
Geodynamic setting
The Jinshachang Pb–Zn deposit
Yangtze Block
Southwest China

ABSTRACT

The Jinshachang Pb–Zn deposit, an exceptionally radiogenic Pb-enriched sulfide deposit, hosted by dolostone of the Upper Sinian (Neoproterozoic) Dengying Formation and the Lower Cambrian Meishucun Formation, is located in the western Yangtze Block, about 300 km northeast of Kunming city in southwest China. Ore bodies in this deposit are dominated by strata-bound type and steeply dipping vein type. Primary ores in these two types are composed of sphalerite, galena, fluorite, barite and quartz with massive, banded, veined and disseminated structures. Twenty-seven ore bodies in the Jinshachang deposit host 4.6 million tons of sulfide ores at average grades of 4.07 wt.% Pb and 5.03 wt.% Zn. Quartz separates from the sulfide ores have δD_{H2O} values ranging from −137‰ to −86.2‰ with an average of −114‰ ($n = 7$), lower than those of magmatic, metamorphic and meteoric water, suggesting a contribution of organic water. $\delta^{34}S_{CDT}$ values of ninety-one sulfide separates range from +1.1‰ to +13.4‰ with an average of +5.7‰, lower than those of evaporites ($\delta^{34}S_{CDT}$ = +15‰ to +35‰) in the Cambrian to Triassic sedimentary strata in NE Yunnan province. $\delta^{34}S_{CDT}$ values of eight barite separates range from +32‰ to +35‰ (average +34‰), within the range of evaporites. These data suggest that S^{2-} in the hydrothermal fluids derived from evaporites by thermo-chemical sulfate reduction (TSR), whereas SO_4^{2-} directly originated from the evaporites. Six sulfide separates have highly radiogenic $^{206}Pb/^{204}Pb$ ratios ranging from 20.74 to 21.18 (average 20.92), $^{207}Pb/^{204}Pb$ ratios ranging from 15.85 to 15.89 (average 15.87), and $^{208}Pb/^{204}Pb$ ratios ranging from 40.89 to 41.42 (average 41.16). The Pb isotopes of the sulfides plot above the upper crust Pb average evolution curve and overlap the Cambrian sedimentary rocks, but are different from the Sinian dolostone. This indicates a crustal source of Pb most likely derived from the Cambrian sedimentary rocks. The initial $^{87}Sr/^{86}Sr$ ratio of seven main stage sphalerite separates from the Jinshachang deposit is 0.713, which is higher than those of the Upper Sinian Dengying Formation dolostone (0.708–0.710), Lower Cambrian carbonates (0.708–0.710), Devonian to Lower Permian sedimentary rocks (0.707–0.711) and Middle Permian Emeishan flood basalts (0.704–0.708), and lower than those of the Proterozoic folded basement rocks (0.724–0.729), but similar to those of Lower Cambrian black shale (0.712–0.714). Therefore, the Sr isotope data of the sphalerite support the view that the Lower Cambrian sedimentary rocks, in particular the black shale, were important source of metals. The main stage sphalerite separates have an Rb–Sr isotopic age of 206.8 ± 3.7 Ma, reflecting the timing of Pb–Zn mineralization. This study suggests that the Jinshachang Pb–Zn deposit is an epigenetic, thrust fold-controlled and strata-bound deposit with fluids and metals derived from the Cambrian sedimentary strata.

1. Introduction

Carbonate-hosted Pb–Zn deposits, an important sub-type of sediment-hosted Pb–Zn deposits, are widely distributed around the world (Leach et al., 2005, 2010). The most representative deposits occur in North America (e.g., Brannon et al., 1992) and Central Europe (e.g., Heijlen et al., 2003; Muchez et al., 2005). In the western Yangtze Block (Fig. 1A), southwest China, 408 carbonate-hosted Pb–Zn deposits are distributed in a large triangular area of 170,000 km^2 in NE Yunnan, NW Guizhou and SW Sichuan provinces (Zheng and Wang, 1991; Cromie et al., 1996; Liu and Lin, 1999; Zhou et al., 2001; Huang et al., 2004; Han et al., 2007a;

* Corresponding author at: State Key Laboratory of Ore Deposit Geochemistry, Institute of Geochemistry, Chinese Academy of Sciences, Guiyang 550002, China.
E-mail address: zhoujiaxi@vip.gyig.ac.cn (J.-X. Zhou).

http://dx.doi.org/10.1016/j.jseaes.2014.11.024
1367-9120/

Zaw et al., 2007; Zhang et al., 2014). They form the famous Sichuan–Yunnan–Guizhou (SYG) Pb–Zn metallogenic province (Huang et al., 2003, 2010; Han et al., 2007b; Zhou et al., 2013a, 2014a). This province contains total Pb + Zn ore reserves of more than 150 million tons (Mt) at an average grades of 5 wt.% Pb and 10 wt.% Zn (Zhou et al., 2011, 2013a, 2013b), making it a major source of base metals in China (Liu and Lin, 1999; Huang et al., 2010; Zhou et al., 2014b). The largest Pb–Zn deposits include the Daliangzi (Zheng and Wang, 1991), Huize (Han et al., 2007a; Li et al., 2007; Yin et al., 2009; Huang et al., 2010), Maoping (Han et al., 2007b) and Tianbaoshan (Zhou et al., 2013c). Despite some recently published studies (Huang et al., 2010; Ye et al., 2011; Bai et al., 2013; Wu et al., 2013; Zhou et al., 2013a, 2013b, 2013c, 2013d, 2013e, 2014a, 2014b; Zhang et al., 2014), there are still many unknown aspects regarding the source of hydrothermal fluids, ore genesis, and geodynamic setting of the Pb–Zn deposits in the SYG province (Zhou et al., 2014a; Zhang et al., 2014). The Jinshachang Pb–Zn deposit, an exceptionally radiogenic Pb-enriched sulfide deposit (Liu, 1989; Liu and Lin, 1999; Bai et al., 2013), is located in the central part of the SYG province on the western Yangtze Block, southwest China (Fig. 1B). This deposit is hosted by dolostone of the Upper Sinian Dengying Formation and the Lower Cambrian Meishucun Formation, and is structurally controlled by the Jinshachang thrust fault and anticline (Figs. 2A–C; Bai et al., 2013; Zhang et al., 2014). In addition, this deposit also shows some unique features (Table 1) that include (i) the barite, fluorite and quartz are common and co-exist with sulfides, (ii) the organic matters are widespread and are closely associated with sulfides, and (iii) the ore-forming fluids have low salinity (2–11 wt.% NaCl) and medium temperature (114–290 °C). Therefore, the Jinshachang deposit is used as a case study.

Isotopes are powerful for determining the origin of ore-forming fluids and metals. For example, H–O and S isotopes have been widely used to constrain the source of hydrothermal fluids (e.g., Seal, 2006; Basuki et al., 2008; Zhou et al., 2010), and Pb and Sr isotopes are useful for tracing the origin of ore-forming metals (e.g., Carr et al., 1995; Deng et al., 2000; Mirnejad et al., 2011; Gromek et al., 2012; Zhou et al., 2013a, 2013b; Dou et al., 2014). Several studies have explored the application of the Rb–Sr isotopic system to determine the age of hydrothermal mineral deposition (e.g., Brannon et al., 1992; Nakai et al., 1993; Christensen et al., 1995; Li et al., 2005; Zhou et al., 2013a). In this paper, we describe the geology of the Jinshachang deposit in detail and report H–O isotopic data of quartz, Rb–Sr isotopic age of main stage sphalerite, and Pb isotopic data of sulfides and country rocks. This new dataset, together with the previously published results, is used to understand the origin of ore-forming fluids and metals, and the ore-forming geodynamic setting of the Jinshachang deposit. These results are also used to discuss the causes of highly concentrated base metals in the SYG province.

2. Geological setting

2.1. Regional geology

South China is made up of the Yangtze Block in the north and the Cathaysian Block in the south (Fig. 1A). The Yangtze Block consists of Archean crystalline basement, Meso- to Neoproterozoic folded basement and Paleozoic to Mesozoic cover sequence (Liu and Lin, 1999; Qiu et al., 2000; Zhou et al., 2002a; Wang et al., 2014). In the western Yangtze Block, the folded basement includes the Dongchuan (~1.7 to ~1.5 Ga) and Kunyang/Huili (~1.2 to ~0.9 Ga) Groups and equivalents (Sun et al., 2009; Zhao et al., 2010) that consist of greywacke, slate and other carbonaceous and siliceous sedimentary rocks. These rocks are unconformably overlain by shallow marine Paleozoic and Early Mesozoic cover sequence (Yan et al., 2003). Evaporites and organic matters are common in Cambrian to Triassic sedimentary strata (Bai et al., 2013; Wu et al., 2013; Zhou et al., 2014a, 2014b). Late Mesozoic (Cretaceous) to Cenozoic lithologies are composed entirely of a continental sequence (Liu and Lin, 1999). A major feature of the western Yangtze Block is the Permian (ca. ~260 Ma) Emeishan Large Igneous Province and its flood basalts that cover an area of more than 250,000 km^2 (Zhou et al., 2002b). After eruption of the Emeishan basalts, the western Yangtze Block collided with the adjacent Yidun arc resulting in closure of the Paleo-Tethys Ocean (Reid et al., 2007; Zhou et al., 2013a, 2013b, 2013c, 2013d). This event is known as the Indosinian Orogeny (Hu and Zhou, 2012; Mao et al., 2012), which forms the main thrust faults and folds in the western Yangtze Block (Fig. 1B). Tectonics, magma and ore deposits formed in the Indosinian in the western Yangtze Block

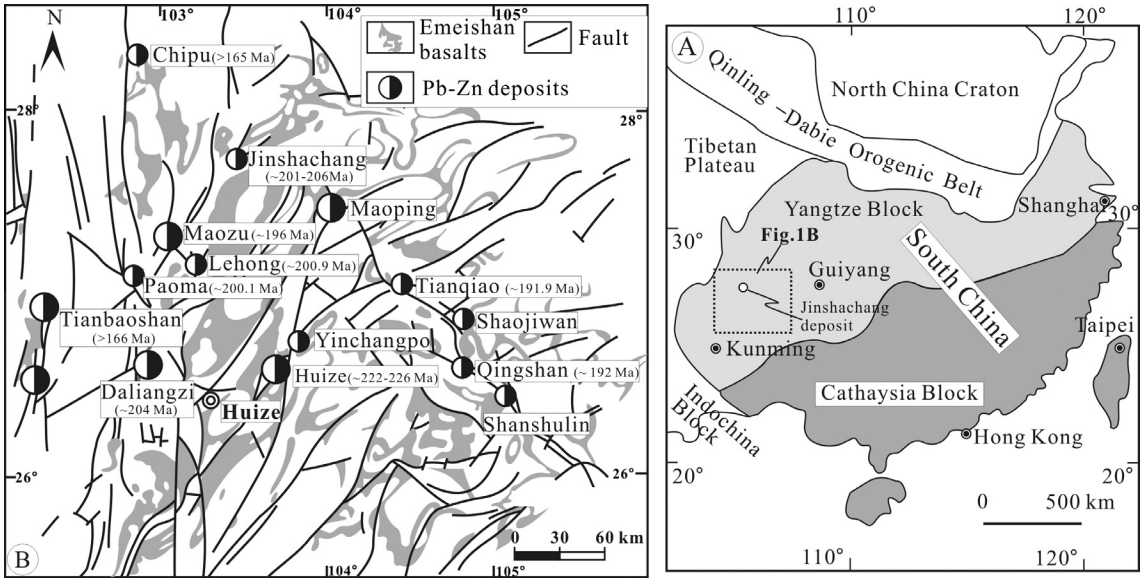

Fig. 1. (A) Tectonic map of South China; (B) regional geological map of the Sichuan–Yunnan–Guizhou Pb–Zn metallogenic province (modified from Liu and Lin, 1999). Ages are from Li et al. (2007), Yin et al. (2009), Lin et al. (2010), Mao et al. (2012), Wang et al. (2012), Wu (2013), Zhou et al. (2013a, 2013d) and Zhang et al. (2014) and this paper.

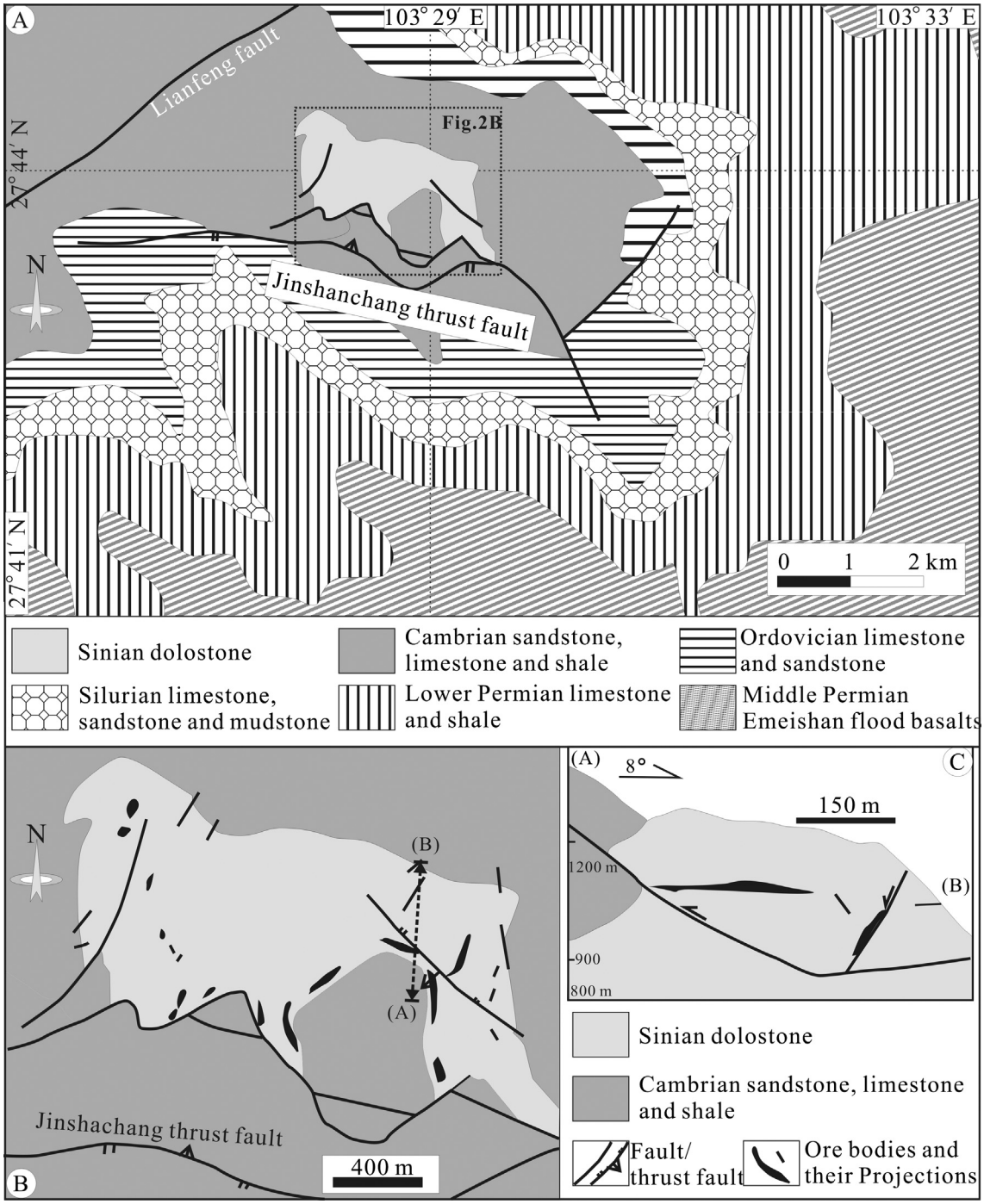

Fig. 2. (A) Geological map of the Jinshachang area (modified from Bai et al., 2013); (B) geological map of the Jinshachang deposit (modified from Zhang et al., 2014); (C) A–B cross section of the Jinshachang deposit (modified from Zhang et al., 2014).

have been affected by the later Yanshanian and Himalayan orogenic events (Liu and Lin, 1999; Zaw et al., 2007; Pirajno, 2013; Zhou et al., 2014b).

Many Pb–Zn deposits have been reported in the SYG province, which are characterized by irregular ore bodies with simple mineralogy, weak wall rock alteration, high grades of Pb + Zn, and associated with useful Ag, Ge, Cd and Ga (Zheng and Wang, 1991; Han et al., 2007a, 2007b; Zhou et al., 2011, 2014a; Bai et al., 2013; Zhang et al., 2014). These deposits are hosted in Neoproterozoic (Sinian) to Lower Permian carbonate rocks that are all overlain by Middle Permian Emeishan flood basalts (Zheng and Wang, 1991; Liu and Lin, 1999; Deng et al., 2000; Zhou et al., 2001; Han et al., 2007a, 2007b; Huang et al., 2010). Main faults in the eastern part of the SYG province trend NW (Fig. 1B; Zhou et al., 2013a), whereas NS- and NE-trending faults are dominant in the western part (Fig. 1B; Han et al., 2007a; Zhou et al., 2013d). It is evident that these regional faults strictly control the distribution of Pb–Zn deposits in the SYG province (Fig. 1B; Liu and Lin, 1999; Han et al., 2007a, 2007b; Zhou et al., 2013a, 2013b, 2013c, 2013d, 2013e). The SYG province can be divided into three parts according to the geographic positions: (i) the northwest SYG province (Sichuan), (ii) the southwest SYG province (Yunnan), and (iii) the southeast SYG province

Table 1
Host rocks, ore-forming elements and ages for the majority Pb–Zn deposits in the SYG province and typical MVT deposits.

Position	Deposit	Host rock	Ore-controlling structure	Metal association	Tonnage, grade	Salinity, temperature	Age, method	Source
Northwest SYG province (Sichuan)	Daliangzi	Sinian dolostone	NW-trending thrust faults	Zn–Pb–Ge–Cd–Ga–Ag	4.5 Mt, 10–12 wt.%	18 wt.% NaCl, 170–225 °C	204.4 ± 1.2 Ma, Calcite Sm–Nd	Zheng and Wang (1991) and Wu (2013)
	Tianbaoshan	Sinian dolostone	NNE-trending thrust faults	Zn–Pb–Cd–Ag–Cu	2.6 Mt, 10–15 wt.%	12.4–20 wt.% NaCl, 157–267 °C	>166 Ma, Zircon U–Pb	Wang et al. (2012) and Zhou et al. (2013c)
	Chipu	Sinian dolostone	NW- and NE-trending thrust-fold	Zn–Pb–Ga–Ge–Ag	0.65 Mt, 10.4 wt.%	8.5–17 wt.% NaCl, 130–250 °C	>165.7 ± 9.9 Ma, Asphalt Re–Os	Wu (2013) and Wu et al. (2013)
	Paoma	Sinian–Cambrian dolostone	NNE-trending thrust-fold	Zn–Pb–Ag	>0.2 Mt, >10 wt.%	118–184 °C	200.1 ± 4 Ma, Sphalerite Rb–Sr	Lin et al. (2010)
Southwest SYG province (Yunnan)	Maozu	Sinian dolostone	NE-trending thrust-fold	Zn–Pb–Cd–Ag	2 Mt, 12–14 wt.%	2.8–5.3 wt.% NaCl, 153–248 °C	196 ± 13 Ma, Calcite Sm–Nd	Zhou et al. (2013d)
	Lehong	Sinian dolostone	NW-trending thrust faults	Zn–Pb–Ag	2.4 Mt, >15 wt.%	11.3–14.5 wt.% NaCl, 165–229 °C	200.9 ± 2.3 Ma, Sphalerite Rb–Sr	Mao et al. (2012) and Wu (2013)
	Jinshachang	Sinian–Cambrian dolostone	NWW-trending thrust-fold	Zn–Pb–Ag	0.42 Mt, 9.1 wt.%	2–11 wt.% NaCl, 114–290 °C	≃201–206 Ma, Fluorite Sm–Nd and sphalerite Rb–Sr	Mao et al. (2012) and Zhang et al. (2014); this paper
	Maoping	D–C, dolostone	NE-trending thrust-fold	Zn–Pb–Ge–Ga–Cd–Ag	3 Mt, >25 wt.%	6.7–13.8 wt.% NaCl, 123–206 °C	No data	Han et al. (2007b)
	Huize	C, dolostone	NE-trending thrust faults	Zn–Pb–Ge–Cd–Ag	7 Mt, >25 wt.%	6–12 wt.% NaCl, 165–220 °C	~222–226 Ma, Calcite Sm–Nd and sphalerite Rb–Sr	Zhou et al. (2001), Han et al. (2007a), Li et al. (2007) and Yin et al. (2009)
Southeast SYG province (Guizhou)	Tianqiao	D–C, dolostone	NW-trending thrust-fold	Zn–Pb–Cd–Ag–Ge	0.4 Mt, 15–18 wt.%	9.6–14.2 wt.% NaCl, 150–270 °C	191.9 ± 6.9 Ma, Sphalerite Rb–Sr	Zhou et al. (2013a)
	Shaojiwan	D, dolostone	NW-trending thrust-fold	Zn–Pb–Cd–Ag	0.5 Mt, 15–20 wt.%	0.9–17.5 wt.% NaCl, 115–170 °C	No data	Zhou et al. (2013b)
	Qingshan	C, dolostone	NW-trending thrust faults	Zn–Pb–Cd–Ag	>0.3 Mt, >15 wt.%	6.3–10.5 wt.% NaCl, 110–276 °C	~192 Ma, Pb isotope model age	Zhou et al. (2013e)
	Shanshulin	C, dolostone	NW-trending thrust faults	Zn–Pb–Cd–Ag	>0.5 Mt, >15 wt.%	<15 wt.% NaCl, 150–280 °C	No data	Zhou et al. (2014b)
North America	Typical MVT deposits	Cambrian to C, carbonates	Extensional setting	Zn–Pb–Ag–(Cu)	<1 Mt, <10 wt.%	10–30 wt.% NaCl, 50–200 °C	Proterozoic to Cretaceous	Leach et al. (2005, 2010)

D = Devonian, C = Carboniferous. Tonnage is Pb + Zn metal reserve. Grade is ore grade of Pb + Zn.

(Guizhou). There is a trend that the strata that host Pb–Zn ores in the northwestern part of the SYG province (Sinian to Cambrian) are older than those in the southeastern part (Devonian to Carboniferous) (Table 1; Zhou et al., 2013a, 2013b, 2013c, 2013d; Zhang et al., 2014).

In the southwestern SYG province, there are about 160 Pb–Zn deposits distributed along NS- and NE-trending faults (Fig. 1B). The cover sequences above the Proterozoic folded basement include the Upper Sinian Dengying Formation and Paleozoic sedimentary sequences, and Emeishan flood basalts (Zheng and Wang, 1991; Zhou et al., 2001; Huang et al., 2003, 2010; Han et al., 2007a). These deposits are hosted in carbonate rocks of Upper Sinian, Cambrian, Devonian, Carboniferous and Lower Permian strata (Liu and Lin, 1999; Deng et al., 2000; Han et al., 2007a; Zhou et al., 2013d; Zhang et al., 2014), of which the Upper Sinian and Carboniferous strata are the two main hosting strata (Table 1). Among these deposits, there are three large Pb–Zn–Ag deposits, namely the Maozu Zn–Pb deposit (Zhou et al., 2013d), the Maoping Zn–Pb–Ge deposit (Han et al., 2007b) and the Lemachang Ag–Pb–Zn deposit (Deng et al., 2000), and one world-class deposit named the Huize Zn–Pb–Ge deposit (Zhou et al., 2001; Han et al., 2007a; Huang et al., 2004). The studied Jinshachang deposit is located in the northern part of the southwestern SYG province (Fig. 1B) and is a representative medium-size Pb–Zn sulfide deposit (Bai et al., 2013; Zhang et al., 2014).

Previous studies in the SYG province have reported hydrothermal calcite/fluorite Sm–Nd isochron ages of the Huize, Maozu and Jinshachang Pb–Zn deposits at 222 ± 14 Ma (Li et al., 2007), 196 ± 13 Ma (Zhou et al., 2013d) and 201 Ma (201.1 ± 2.9 Ma: Mao et al., 2012; 201.1 ± 6.2 Ma: Zhang et al., 2014), respectively, and Rb–Sr isochron ages of sulfide minerals (sphalerite and/or pyrite) for the Paoma, Tianqiao, Lehong and Jinshachang Pb–Zn deposits at 200.1 ± 4.0 Ma (Lin et al., 2010), 191.9 ± 6.9 Ma (Zhou et al., 2013a), 200.9 ± 2.3 Ma (Mao et al., 2012) and 200.9 ± 8.3 Ma (Zhang et al., 2014), respectively. Thus, the Pb–Zn mineralization in the SYG province formed in the Late Triassic to Early Jurassic (222–192 Ma). The Pb–Zn mineralization in the SYG province is linked to the late Indosinian Orogeny that formed in response to the closure of the Paleo-Tethys Ocean (Hu and Zhou, 2012; Mao et al., 2012; Zhou et al., 2013a, 2014b; Zhang et al., 2014). This suggests a convergent ore-forming geodynamic setting.

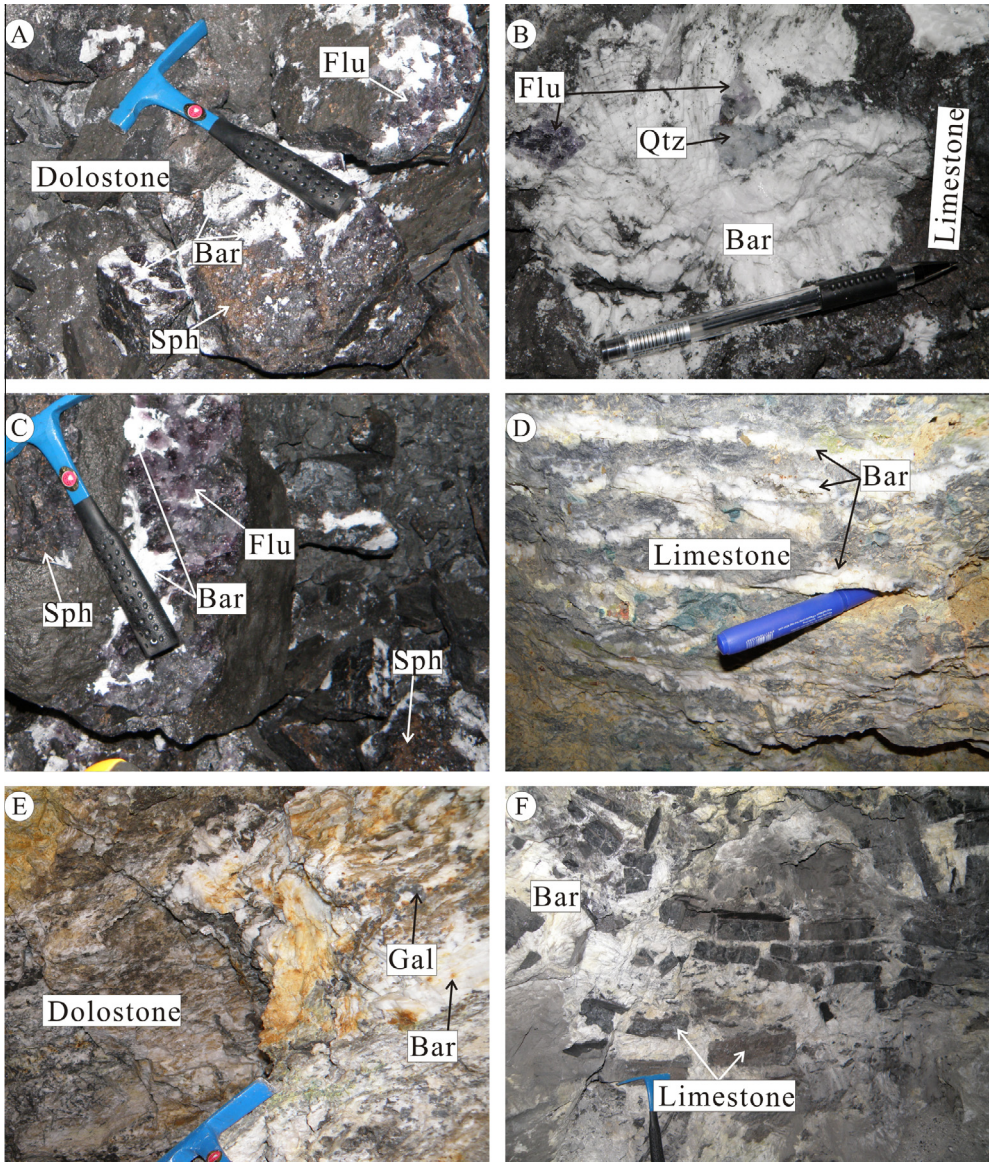

Fig. 3. Ore field photos of the Jinshachang deposit. (A) Disseminated sphalerite (Sph) with patchy barite (Bar) and fluorite (Flu) in dolostone; (B) Patchy quartz (Qtz) and Flu enclosed in radial Bar; (C) Vein Flu and Bar and patchy Sph; (D) Vein Bar in limestone; (E) disseminated galena (Gal) and patchy Bar; (F) limestone breccias enclosed in Bar.

2.2. Geology of the Jinshachang deposit

Ore bodies in the Jinshachang deposit are hosted in dolostone of the Upper Sinian Dengying Formation and phosphorous dolostone of the Lower Cambrian Meishucun Formation, and are structurally controlled by the NWW–SEE-trending Jinshachang anticline and the NW–SE-trending Jinshachang thrust fault (Figs. 2A–C). In the Jinshachang ore field, dolostone of the Upper Sinian Dengying Formation, sedimentary rocks (sandstone, phosphorous dolostone, limestone and black shale) of Cambrian to Silurian and Lower Permian, and Middle Permian Emeishan flood basalts formed the Jinshachang anticline (Fig. 2A). The axial trend of the Jinshachang anticline is 285° (Liu, 1989).

Twenty-seven ore bodies are delineated in the upper part of the Dengying Formation (Fig. 2B), of which individual ore bodies are 72–665 m long, 137–175 m wide and 1.04–6.03 m thick, with 1.56–7.14 wt.% Pb, 2.16–10.76 wt.% Zn and 14.1–128.3 g/t Ag (Bai et al., 2013). The average Pb/Zn ratio is 0.8. Ore bodies occur dominantly as strata-bound type (dip at 5–25°) within the interlayer fracture zones in the northeastern and southwestern limbs of the NWW–SEE trending Jinshachang anticline (Zhang et al., 2014) and steeply dipping veins along the secondary faults (Fig. 2C). Ore reserves of all the sulfide ore bodies are about 4.6 million tons at an average grades of 4.07 wt.% Pb and 5.03 wt.% Zn.

Nos. I and IV ore bodies are strata-bound. No. I ore body occurs along the interlamination fracture zone of the Dengying Formation (Fig. 2C). It is 100–330 m long, 65–246 m wide and 1.65–5.29 m thick, with an average grade of 8.74 wt.% Pb, 4.14 wt.% Zn and 97.2 g/t Ag. Nos. II, III and V ore bodies occur as steeply dipping veins. No. II ore body occurs along the secondary fracture of the Jinshachang thrust fault (Fig. 2C). It is 100 m in length, average 80 m in width and 5.5 m thick at average, with 1.14–3.11 wt.% Pb, 3.06–6.82 wt.% Zn and 22.7–51.5 g/t Ag. Ore bodies of this type trend dominantly 70–84° (Fig. 2C; Bai et al., 2013).

Ores in the Jinshachang deposit underwent hydrothermal and supergene oxidizing processes (Bai et al., 2013; Zhang et al., 2014). Therefore, there are oxidized and unaltered sulfide ores along with a mixture of these two types. Unaltered sulfide ores are composed of sphalerite, galena, barite, fluorite and quartz, with a small number of dolostone and calcite (Bai et al., 2013; Zhang

et al., 2014). Oxidized and mixed ores have extremely complex assemblages of smithsonite, limonite, cerusite, sulfide, quartz, fluorite, and barite and carbonate minerals. The sulfide ores are dominated by massive, vein-type and disseminated structures, and the minerals display textures of anhedral to euhedral granular, filling and pressure shadows (Figs. 3 and 4; Bai et al., 2013; Zhang et al., 2014).

Based on crosscutting, overgrowth and replacement relationships, the hydrothermal period is divided into three stages (Table 2): (I) the pyrite-silicified dolostone stage (Fig. 4E), (II) the sulfide–barite–fluorite–quartz stage, and (III) the barite–fluorite–quartz stage (Fig. 3B, D and F). Stage II is the main stage and has the mineral assemblages of sphalerite–fluorite (Fig. 4A), sphalerite–barite (Fig. 4B), sphalerite–barite–fluorite (Fig. 3A and C), sphalerite–galena–barite–fluorite (Fig. 4C), sphalerite–galena–quartz (Fig. 4F) and galena–barite/fluorite (Figs. 3E and 4D).

Wall rock alterations are simple and include silicification, fluoritization, baratization and dolomitization (Bai et al., 2013; Zhang et al., 2014), of which dolomitization enhances rock brittleness and causes crack opening for Pb–Zn mineralization.

3. Analytical methods

3.1. H–O isotope analysis

Quartz separates from different stages were analyzed on a Finnegan MAT-253 mass spectrometer. $\delta^{18}O$ values were obtained by using the conventional fluorination method and H isotope analysis was carried out by thermal decrepitation on fluid extracted from inclusions in quartz samples (Clayton and Mayeda, 1963). Results are reported to Vienna Standard Mean Ocean Water (V-SMOW) with analytical precisions of ±1‰ for δD value and ±0.5‰ for $\delta^{18}O$ value. The $\delta^{18}O$ value of H_2O in fluid inclusions was calculated by using the quartz-water fractionation equation described by Clayton et al. (1972).

3.2. Pb isotope analysis

Pb isotope analysis was carried out using a GV Isoprobe-T Thermal Ionization Mass Spectrometer (TIMS) at Beijing Institute of Uranium Geology. The analytical procedures involved dissolution

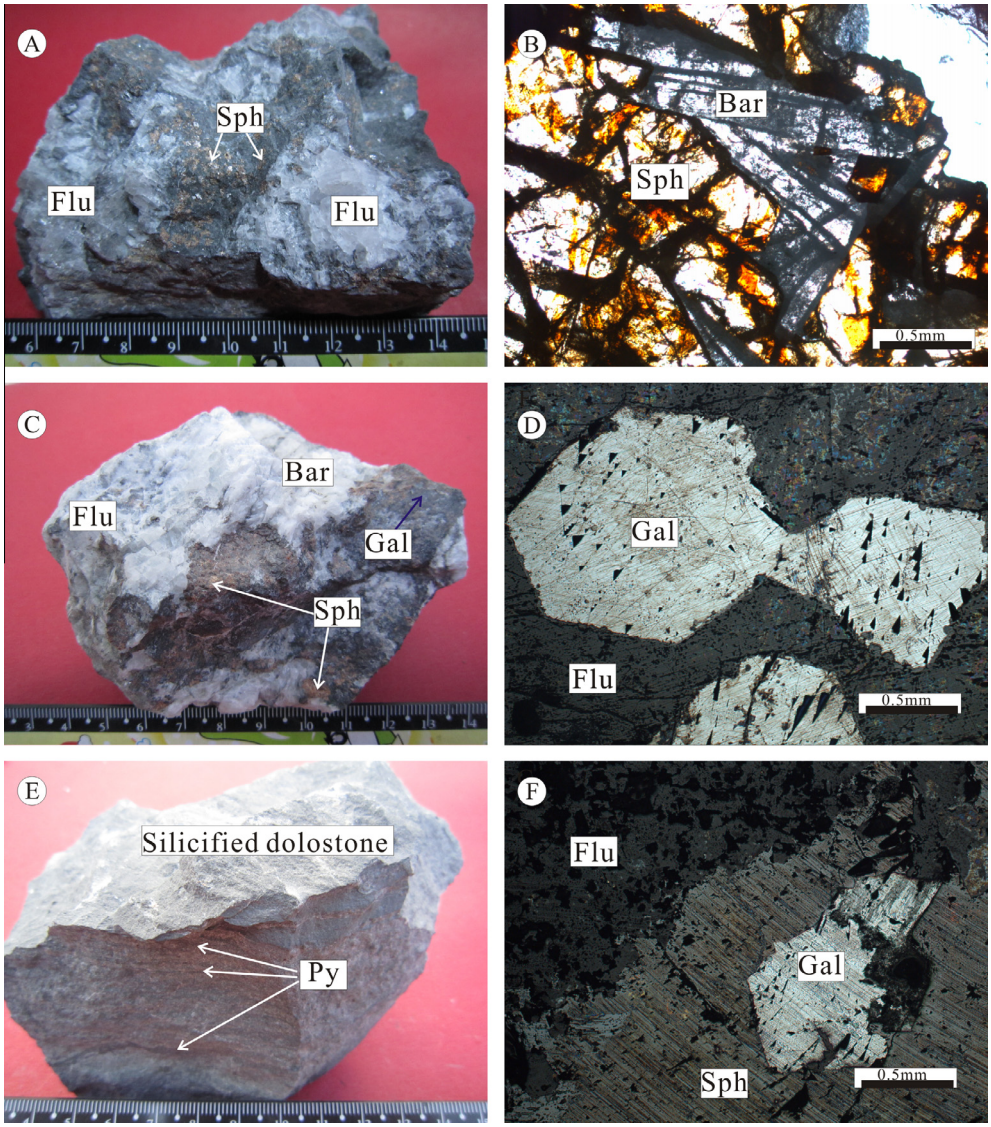

Fig. 4. Pictures of ores and microscope reflected light photographs of sulfide ores from the Jinshachang deposit. (A) Vein sphalerite (Sph) and aggregate fluorite (Flu); (B) granular Sph enclosed in vein barite (Bar); (C) granular aggregate Sph with disseminated galena (Gal) and aggregate Flu and Bar; (D) pressure shadow of granular Gal enclosed in Flu; (E) banded pyrite enclosed in silicified dolostone; (F) pressure shadow of granular Gal enclosed in Sph.

Table 2
Mineral paragenesis of the Jinshachang deposit.

Period	Hydrothermal			Supergene
Stage	Stage I	Stage II	Stage III	Stage IV
Mineral assemblage	Pyrite-silicified dolostone	Sulfide-barite-fluorite-quartz	Barite-fluorite-quartz	Oxidized mineral
Pyrite	—	—	—	
Sphalerite		—		
Galena		—		
Barite		—	—	
Fluorite		—	—	
Quartz	—	—	—	
Dolomite	—	—	—	
Calcite	—	—	—	
Limonite				—
Cerusite				—
Smithsonite				—

— Less; ▬ More, after Bai et al. (2013) and Zhang et al. (2014).

of samples using HF and $HClO_4$ in crucibles, followed by basic anion exchange resin to purify Pb (Belshaw et al., 1998). Analytical results for NBS 981 are $^{206}Pb/^{204}Pb = 16.937 \pm 0.003$ ($2\sigma_m$), $^{207}Pb/^{204}Pb = 15.457 \pm 0.003$ ($2\sigma_m$) and $^{208}Pb/^{204}Pb = 36.6$ 11 ± 0.005 ($2\sigma_m$).

3.3. Rb–Sr isotope analysis

Chemical separation of Rb and Sr from matrix elements and mass spectrometric measurements were accomplished at Chinese Academy of Sciences. Spec-Sr exchange resin was used for the separation and purification of Rb and Sr. The procedure blanks of Rb and Sr are about 6 and 5 pg (10^{-12} g), respectively. A detailed analytical procedure for Rb–Sr isotope analysis is available in Li et al. (2005). Rb–Sr isotopic compositions were measured by the GV Isoprobe-T TIMS. An $^{88}Sr/^{86}Sr$ ratio of 8.37521 is used to calibrate mass fractionation of Sr isotope. The average $^{87}Sr/^{86}Sr$ ratio of NBS 987 is 0.710242 ± 5 ($2\sigma_m$). The uncertainties ($2\sigma_m$) are 0.005% for $^{87}Sr/^{86}Sr$ ratio and 2% for $^{87}Rb/^{86}Sr$ ratio.

4. Results

4.1. H and O isotopic compositions

H–O isotopic compositions of fluid inclusions in quartz are listed in Table 3 and shown in Fig. 5. The ore-forming temperatures range from 114 to 290 °C based on micro-thermometric data of fluid inclusions in quartz and fluorite from Bai et al. (2013). $\delta^{18}O_{H2O} = \delta^{18}O_{quartz} - 3.38 \times 10^6/(t + 273.15)^2 + 3.40$ (Clayton et al., 1972). Fluid inclusions in quartz have δD_{H2O} values ranging from −137‰ to −86.2‰ (average −114‰) and $\delta^{18}O_{H2O}$ values (calculate base on average temperatures of Stages I to III) ranging from +5.7‰ to +8.4‰ (average +7.1‰). One Stage I quartz separate (average t = 260 °C) has δD_{H2O} value of −86.2‰ and $\delta^{18}O_{H2O}$ value of +7.1‰. The δD_{H2O} and $\delta^{18}O_{H2O}$ values for Stage II quartz separates (average t = 220 °C) range from −116‰ to −109‰ (mean −112‰, n = 4) and from +6.9‰ to +8.4‰ (mean +7.6‰, n = 4), respectively. Two Stage III quartz separates (average t = 180 °C) have δD_{H2O} and $\delta^{18}O_{H2O}$ values ranging from −137‰ to −125‰ (average −131‰) and +5.7‰ of +6.5‰ (average +6.1‰), respectively. It is clear that the δD_{H2O} values of Stages I to III quartz samples decrease, whereas the $\delta^{18}O_{H2O}$ values do not change regularly (Fig. 5).

4.2. Pb isotopic compositions

Lead isotopic compositions of sulfide separates from the Jinshachang deposit and the country rocks are listed in Table 4 and shown in Fig. 6. Two Stage I pyrite separates have $^{206}Pb/^{204}Pb$, $^{207}Pb/^{204}Pb$ and $^{208}Pb/^{204}Pb$ ratios ranging from 20.741 to 20.768, 15.849 to 15.867 and 40.888 to 40.909, respectively. $^{206}Pb/^{204}Pb$, $^{207}Pb/^{204}Pb$ and $^{208}Pb/^{204}Pb$ ratios of two Stage II sphalerite separates range from 20.805 to 21.177, 15.875 to 15.884 and 41.017 to 41.359, respectively. Two Stage II galena separates have $^{206}Pb/^{204}Pb$ ratios ranging from 21.009 to 21.020, $^{207}Pb/^{204}Pb$ ratios ranging from 15.877 to 15.887 and $^{208}Pb/^{204}Pb$ ratios ranging from 41.387 to 41.421. It is obvious that Stage II sulfide samples contain more radiogenic Pb than Stage I and galena contains similar radiogenic Pb to sphalerite. Four Cambrian sedimentary rocks (carbonates and black shale) have $^{206}Pb/^{204}Pb_{206\ Ma}$, $^{207}Pb/^{204}Pb_{206\ Ma}$ and $^{208}Pb/^{204}Pb_{206\ Ma}$ ratios ranging from 20.950 to 22.354, 15.837 to 15.930 and 40.878 to 41.928, respectively (Table 4), higher than those of Upper Sinian dolostone ($^{206}Pb/^{204}Pb_{206\ Ma}$ = 18.235–18.275, $^{207}Pb/^{204}Pb_{206\ Ma}$ = 15.699–15.777, $^{208}Pb/^{204}Pb_{206\ Ma}$ = 38.547–38.809, n = 4).

4.3. Rb–Sr isotopic compositions and isochron age

The main stage sphalerite separates in the Jinshachang Pb–Zn deposit are analyzed for Rb–Sr isotopic compositions (Table 5). Rb and Sr contents of seven sphalerite separates range from 0.296 to 1.35 × 10^{-6} (10^{-6} = ppm) and 3.58 to 319 ppm, respectively. These samples have $^{87}Rb/^{87}Sr$ ratios ranging from 0.021 to 0.485. $^{87}Sr/^{86}Sr$ ratios of seven sphalerite separates are relatively homogeneous and range from 0.7132 to 0.7146. The analyses yield an Rb–Sr isochron age of 206.8 ± 3.7 Ma, with an initial $^{87}Sr/^{86}Sr$ ratio of 0.7131 ± 0.0001 and MSWD of 4.7 (Fig. 7A).

5. Discussion

5.1. Timing of Pb–Zn mineralization

Previous studies demonstrated that Rb–Sr isotopic dating is feasible for certain sulfide minerals (e.g., Brannon et al., 1992; Nakai et al., 1993; Christensen et al., 1995; Christensen and Halliday, 1995; Li et al., 2005). For example, sphalerite may host Rb in its lat-

Table 3
H–O isotopic compositions of quartz separates from the Jinshachang deposit.

No.	Object	Stage	$\delta D_{H2O\text{-}SMOW}$ (‰)	$\delta^{18}O_{Qtz\text{-}SMOW}$ (‰)	$\delta^{18}O_{H2O\text{-}SMOW}$ (‰)	Source
105-202-06	Quartz	Stage III	−125	+18.8	+5.7	Bai unpublished
105-202-08	Quartz	Stage III	−137	+19.6	+6.5	
889-02	Quartz	Stage II	−114	+17.6	+7.1	
889-04	Quartz	Stage I	−86.2	+15.6	+7.1	
889-05	Quartz	Stage II	−109	+18.9	+8.4	This paper
889-06	Quartz	Stage II	−116	+18.3	+7.8	
889-08	Quartz	Stage II	−109	+17.4	+6.9	
J-4	Quartz		−92.7		−0.1	Liu and Lin (1999)
17	Quartz		−86.9		+2.8	

$10^3 \ln \alpha_{Qtz\text{-}H2O} = \delta^{18}O_{Qtz} - \delta^{18}O_{H2O} = 3.38 \times 10^6/(t + 273.15)^2 - 3.40$ (Clayton et al., 1972); t_I = 260 °C, t_{II} = 220 °C, t_{III} = 180 °C (Bai et al., 2013); Qtz = quartz.

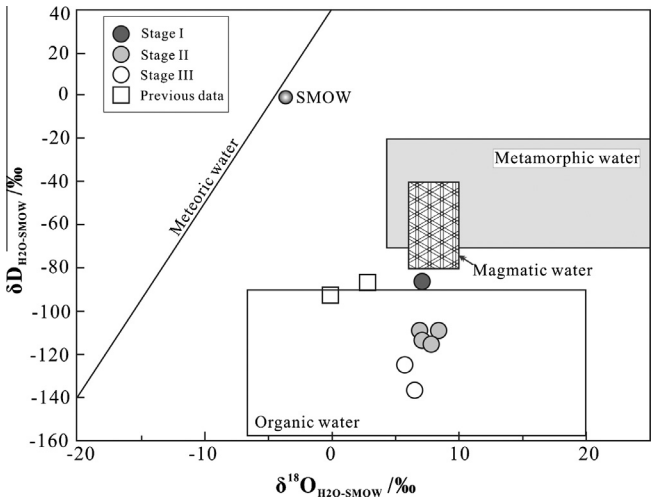

Fig. 5. Diagram of δD_{H2O} *vs.* $\delta^{18}O_{H2O}$ for quartz separates from the Jinshachang deposit.

tice preferentially than Sr, and thus has high $^{87}Rb/^{86}Sr$ ratios, making the mineral suitable for precise radiogenic isotope dating. This method has been applied to hydrothermal deposits (e.g., Brannon et al., 1992; Nakai et al., 1993; Christensen et al., 1995; Christensen and Halliday, 1995; Yin et al., 2009; Mao et al., 2012). A modified single grain Rb–Sr isotopic dating with highly precise TIMS and ultra-low procedural blank is also used for pyrite (Li et al., 2005, 2008) and sphalerite (Lin et al., 2010; Zhou et al., 2013a).

The Rb–Sr isotopic age of 206.8 ± 3.7 Ma for seven main stage sphalerite samples from the Jinshachang deposit is considered to be reliable (Fig. 7A). The fact that 1/Sr values do not co-vary with $^{87}Sr/^{86}Sr$ ratios of samples (Fig. 7B) indicates that the isochron age is not a pseudoisochron and has isochronal meaning (e.g., Nakai et al., 1993; Yin et al., 2009; Zhou et al., 2013a), so this age is interpreted to reflect the timing of the Pb–Zn mineralization. The Rb–Sr isotopic age of sphalerite separates from the Jinshachang deposit is similar to the fluorite Sm–Nd isotopic ages of 201.1 ± 2.9 Ma (Mao et al., 2012) and 201.1 ± 6.2 Ma (Zhang et al., 2014), and is broadly similar to those early reported ages of 222–192 Ma (Li et al., 2007; Lin et al., 2010; Mao et al., 2012; Wu, 2013; Zhou et al., 2013a, 2013d). Therefore, we consider that the Jinshachang deposit formed in the late Indosinian (Late Triassic) related to the closure of the Paleo-Tethys Ocean (Reid et al., 2007; Hu and Zhou, 2012; Zhou et al., 2013a, 2013b, 2013c, 2013d; Zhang et al., 2014).

5.2. Origin of the hydrothermal fluids

5.2.1. Water

Previous studies of two quartz separates have shown the δD_{H2O} values ranging from −92.7‰ to −86.9‰, lower than those of

Table 4
Pb isotopic compositions of sulfides and country rocks from the Jinshachang deposit.

No.	Mineral/rock	Stage	$^{208}Pb/^{204}Pb$	$^{207}Pb/^{204}Pb$	$^{206}Pb/^{204}Pb$	Source
908-4-02	Pyrite	Stage I	40.909	15.867	20.741	Bai unpublished
Jshch16-01	Pyrite	Stage I	40.888	15.849	20.768	
401-7-3-03	Sphalerite	Stage II	41.359	15.875	21.177	
01-7-3-05	Sphalerite	Stage II	41.017	15.884	20.805	
889-03	Galena	Stage II	41.421	15.887	21.020	
889-05	Galena	Stage II	41.387	15.877	21.009	
YJ4-1	Galena		41.790	15.920	21.350	Liu (1989)
PbS-G	Galena		41.124	15.846	20.884	
PbS-J	Galena		41.300	15.888	21.070	
Pb-Y	Galena		41.289	15.856	21.174	
J-4	Galena		41.250	15.847	21.264	
J-10	Galena		41.433	15.879	21.363	
Jshch-1	Cambrian sedimentary rocks		41.441	15.909	21.172	This paper
€1q-01	Cambrian sedimentary rocks		41.928	15.914	22.166	
Z2dn4-01	Cambrian sedimentary rocks		40.878	15.837	20.950	
Z2dn4-02	Cambrian sedimentary rocks		41.028	15.930	22.354	
Dx-3	Sinian dolostone		38.809	15.777	18.275	Liu (1989)
Dx-68	Sinian dolostone		38.738	15.769	18.246	
Bg-4	Sinian dolostone		38.547	15.699	18.245	
Bg-33	Sinian dolostone		38.632	15.719	18.235	

Lead isotopic ratios for sedimentary rocks are age-corrected at 206 Ma. $(^{206}Pb/^{204}Pb)_t = (^{206}Pb/^{204}Pb)_p - \mu(e^{\lambda t} - 1)$, $(^{207}Pb/^{204}Pb)_t = (^{207}Pb/^{204}Pb)_p - \mu/137.88(e^{\lambda' t} - 1)$, $(^{208}Pb/^{204}Pb)_t = (^{208}Pb/^{204}Pb)_p - \omega(e^{\lambda'' t} - 1)$, $\lambda = 1.55125 \times 10^{-10}\ t^{-1}$, $\lambda' = 9.8485 \times 10^{-10}\ t^{-1}$, $\lambda'' = 0.49475 \times 10^{-10}\ t^{-1}$, t = 206 Ma.

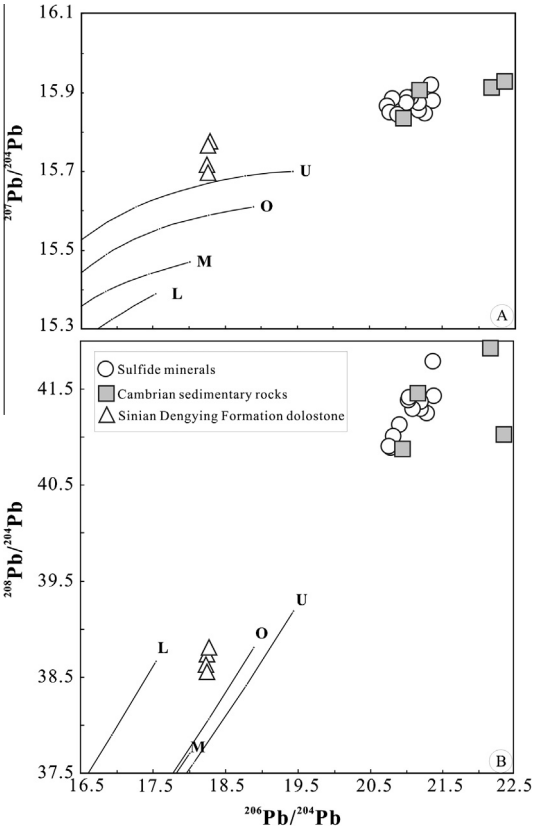

Fig. 6. Plots of $^{207}Pb/^{204}Pb$ *vs.* $^{206}Pb/^{204}Pb$ (A) and $^{208}Pb/^{204}Pb$ *vs.* $^{206}Pb/^{204}Pb$ (B) for sulfides and country rocks from the Jinshachang deposit. U – upper crust; O – orogenic belt; M – mantle; L – lower crust (Zartman and Doe, 1981).

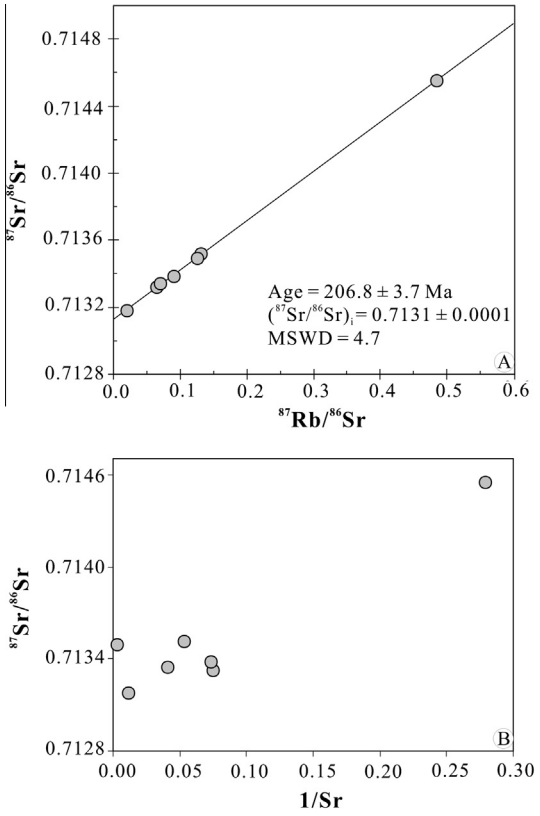

Fig. 7. (A) Rb–Sr isochron for sphalerite separates from the Jinshachang deposit; (B) plot of $1/Sr–^{87}Sr/^{86}Sr$ for the sphalerite separates.

metamorphic (−70‰ to −20‰) and magmatic (−80‰ to −40‰) water (Fig. 5; Zheng and Chen, 2000). Therefore, it is considered that the water in the ore-forming fluids was likely to be a mixture of metamorphic and meteoric water (Liu and Lin, 1999). In this study, we find that the δD_{H2O} values of fluid inclusions in Stage I quartz separates are similar to those of previous data (Table 3; Liu and Lin, 1999), whereas quartz separates of Stages II and III have lower δD_{H2O} values than previous data (Table 3; Fig. 5). On the other hand, all the calculated $\delta^{18}O_{H2O}$ values in this study are higher than previous data within errors (Fig. 5). Organic matters are common in Cambrian sedimentary strata (black shale) and reaction between meteoric and/or metamorphic water with the organic matters will significantly reduce δD_{H2O} values (<−90‰; Zheng and Chen, 2000; Wu et al., 2013). In a δD_{H2O} *vs.* $\delta^{18}O_{H2O}$ diagram (Fig. 5), Stages II and III samples fall into the field of organic water, and Stage I samples plot in the field between metamorphic and organic water. It is clear that in the late stage, organic water becomes more dominated (Fig. 5). This implies that H_2O in the hydrothermal fluids mainly originated from organic water and most likely sourced from the Cambrian organic matters-bearing sedimentary rocks (black shale).

5.2.2. Sulfur

Sulfur isotope geochemistry was systemically studied by Bai et al. (2013). We find that the $\delta^{34}S_{CDT}$ values (Table 6) of ninety-one sulfide samples range from +1.1‰ to +13.4‰ (average +5.7‰), lower than those of evaporites in the Cambrian to Triassic strata (+15‰ to +35‰; Claypool et al., 1980; Liu and Lin, 1999; Seal, 2006; Han et al., 2007a; Bai et al., 2013; Zhou et al., 2013d), whereas the $\delta^{34}S_{CDT}$ values of eight barite samples range from +32.1‰ to +35.2‰ (average +33.9‰), similar to those of evaporites (Fig. 8). These observations suggest that S^{2-} in the hydrothermal fluids was derived from evaporites by thermo-chemical sulfate reduction (TSR), whereas SO_4^{2-} was directly originated from evaporites (Fig. 8; Bai et al., 2013). The formation mechanism of reduced sulfur in the Jinshachang hydrothermal fluids is in agreement with that proposed for the Tianqiao (Zhou et al., 2013a, 2014a) and Huize (Han et al., 2007a) deposits, but the $\delta^{34}S_{CDT}$ values for the sulfides from the Jinshachang deposit are lower than the Tianqiao and Huize deposits (Fig. 8). This suggests that during the TSR process the $\Delta^{34}S$ values between SO_4^{2-} and S^{2-} in different deposits are variable, likely due to varied $\delta^{34}S$ values of evaporites in different hosting strata (Seal, 2006) and/or unequal metallogenic temperatures (Zhou et al., 2013e).

Table 5
Rb–Sr isotopic compositions of sphalerite separates from the Jinshachang deposit.

No.	Object	$Rb/10^{-6}$	$Sr/10^{-6}$	$^{87}Rb/^{87}Sr$	$^{87}Sr/^{86}Sr$	$2\sigma_m$	Source
JS1	Sphalerite	1.35	319	0.125	0.7135	0.0001	This paper
JS2	Sphalerite	0.855	87.2	0.021	0.7132	0.0001	
JS3	Sphalerite	0.670	24.6	0.071	0.7133	0.0001	
JS4	Sphalerite	0.296	13.4	0.065	0.7133	0.0001	
JS5	Sphalerite	0.455	13.6	0.091	0.7134	0.0001	
JS6	Sphalerite	0.590	3.58	0.485	0.7146	0.0001	
JS7	Sphalerite	0.837	18.8	0.132	0.7135	0.0001	

Table 6
S isotopic compositions of sulfides and barite separates from the Jinshachang deposit.

Mineral	$\delta^{34}S_{CDT}$ (‰)	Mineral	$\delta^{34}S_{CDT}$ (‰)	Mineral	$\delta^{34}S_{CDT}$ (‰)
Sphalerite	6.0	Sphalerite	12.3	Sphalerite	4.7
Sphalerite	4.7	Sphalerite	5.6	Galena	6.1
Sphalerite	4.9	Sphalerite	8.6	Galena	6.3
Sphalerite	5.0	Sphalerite	5.3	Galena	7.0
Sphalerite	5.2	Sphalerite	4.8	Galena	8.2
Sphalerite	8.5	Sphalerite	5.0	Galena	3.7
Sphalerite	5.0	Sphalerite	4.8	Galena	8.2
Sphalerite	11.2	Sphalerite	9.1	Galena	6.0
Sphalerite	4.8	Sphalerite	5.8	Galena	6.6
Sphalerite	4.8	Sphalerite	4.5	Galena	7.5
Sphalerite	4.9	Sphalerite	4.4	Galena	6.1
Sphalerite	4.7	Sphalerite	4.7	Galena	7.1
Sphalerite	4.8	Sphalerite	5.7	Galena	9.0
Sphalerite	4.7	Sphalerite	4.7	Galena	9.0
Sphalerite	5.2	Sphalerite	4.7	Galena	8.6
Sphalerite	5.0	Sphalerite	4.3	Galena	7.7
Sphalerite	4.6	Sphalerite	5.2	Galena	7.4
Sphalerite	4.6	Sphalerite	4.0	Galena	3.8
Sphalerite	4.7	Sphalerite	4.2	Galena	7.0
Sphalerite	4.3	Sphalerite	4.6	Galena	1.1
Sphalerite	4.1	Sphalerite	4.1	Galena	4.8
Sphalerite	4.2	Sphalerite	4.0	Galena	2.6
Sphalerite	4.4	Sphalerite	3.6	Galena	4.6
Sphalerite	4.4	Sphalerite	3.9	Galena	5.1
Sphalerite	4.5	Sphalerite	4.0	Galena	2.3
Sphalerite	10.3	Sphalerite	4.1	Barite	34.7
Sphalerite	9.3	Sphalerite	4.1	Barite	33.3
Sphalerite	9.2	Sphalerite	4.2	Barite	32.1
Sphalerite	6.7	Sphalerite	7.0	Barite	35.2
Sphalerite	13.4	Sphalerite	6.5	Barite	34.8
Sphalerite	9.2	Sphalerite	6.5	Barite	32.9
Sphalerite	4.8	Sphalerite	4.7	Barite	34.5
Sphalerite	4.4	Sphalerite	6.1	Barite	34.0

Data are sourced from Bai et al. (2013).

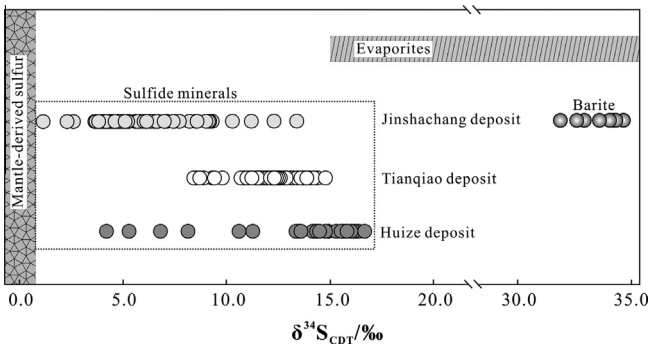

Fig. 8. The $\delta^{34}S_{CDT}$ values for the Jinshachang deposit (Bai et al., 2013) are compared with the Tianqiao (Zhou et al., 2013a, 2014a) and Huize (Han et al., 2007a) deposits, and those of mantle (Chaussidon et al., 1989) and evaporites in the Cambrian to Triassic sedimentary strata (Claypool et al., 1980; Liu and Lin, 1999; Seal, 2006; Han et al., 2007a; Zhou et al., 2013d).

5.3. Possible sources of ore-forming metals

5.3.1. Constraints from Pb isotopes

Because some Pb isotopes are radiogenic, the Pb isotope ratios need to be corrected to a consistent age in order to make comparisons between different phases (e.g., Carr et al., 1995; Muchez et al., 2005; Haest et al., 2010). Sulfides have very low U and Th contents. Hence the radiogenic Pb of sulfides after their formation is negligible and no age correction is needed, whereas the Pb isotopes in the sedimentary rocks are needed. Sphalerite Rb–Sr isotopic dating shows that the age of Pb–Zn mineralization in the Jinshachang deposit is at ca. 206 Ma. Thus, an age of 206 Ma is used to correct Pb isotopic ratios of the country rocks and the age-corrected Pb isotopes are listed in Table 4. In terms of $^{207}Pb/^{204}Pb$ *vs.* $^{206}Pb/^{204}Pb$ and $^{208}Pb/^{204}Pb$ *vs.* $^{206}Pb/^{204}Pb$ ratios (Fig. 6), all sulfide Pb isotope data of the Jinshachang deposit plot above the upper crust Pb evolution curves (Zartman and Doe, 1981), suggesting a crustal source of Pb in the hydrothermal fluids. Moreover, Pb isotopic data for sulfides overlap the Cambrian sedimentary rocks but are different from the dolostone of the Upper Sinian Dengying Formation (Fig. 6). This suggests that the Pb in the ore-forming fluids most likely sourced from the Cambrian sedimentary rocks.

5.3.2. Constraints from Sr isotopes

In order to use Sr isotopes to trace the origin of ore-forming metals, age corrections are also needed (e.g., Fontbote and Gorzawski, 1990; Deng et al., 2000; Zhou et al., 2001; Gromek et al., 2012). Therefore, the 206 Ma sulfide formation age was used to correct $^{87}Sr/^{86}Sr$ ratios of the basement, sedimentary rocks and basalts in the SYG province. The $^{87}Sr/^{86}Sr_{206\ Ma}$ ratios of the Upper Sinian dolostone, Lower Cambrian carbonates and Middle Devonian to Lower Permian sedimentary rocks (carbonates and sandstone) range from 0.7073 to 0.7111 (Table 7; Deng et al., 2000; Shi et al., 2003; Huang et al., 2004; Zhou et al., 2013a, 2013b) and are lower than the initial $^{87}Sr/^{86}Sr$ ratio of sphalerite (0.7131) in the Jinshachang deposit. In addition, the initial $^{87}Sr/^{86}Sr$ of main stage sphalerite is higher than those of Middle Permian basalts (0.7039–0.7078; Huang et al., 2004), but similar to the $^{87}Sr/^{86}Sr_{206\ Ma}$ ratios of Lower Cambrian black shale (0.7120–0.7136; Jiang and Li, 2005). On the other hand, the Proterozoic folded basements have $^{87}Sr/^{86}Sr_{206\ Ma}$ ratios ranging from 0.7243 to 0.7288 (Chen and Ran, 1992; Li and Qin, 1988), significantly higher than the initial $^{87}Sr/^{86}Sr$ ratio of sphalerite separates from the Jinshachang deposit (Fig. 9). Therefore, the Sr of sulfides in the Jinshachang deposit may have a mixed source with the majority most likely sourced from the Cambrian black shale.

5.4. Ore genesis

Ore deposits in the SYG province may have been affected by multiple orogenic events that occurred in the western Yangtze Block (e.g., Zaw et al., 2007). Therefore, the ore genesis of these deposits has long been a matter of debate. For example, it has been proposed that all Pb–Zn deposits in the SYG province were distal magmatic-hydrothermal deposits (Xie, 1963; Xu et al., 2014) associated with the Emeishan basalts, while isotope geochronology studies have suggested that the Pb–Zn mineralization occurred between 222 and 192 Ma (Table 1; Li et al., 2007; Lin et al., 2010; Mao et al., 2012; Wu, 2013; Zhou et al., 2013a, 2013d; Zhang et al., 2014), much younger than the basalts (ca. ~260 Ma; Zhou et al., 2002b). It has also been suggested that these Pb–Zn deposits are comparable to typical MVT-type deposits (e.g., Leach et al., 2005, 2010; Muchez et al., 2005; Pirajno, 2013) in terms of types of host rocks, origin of hydrothermal fluids and tectonic setting (Zheng and Wang, 1991; Zhou et al., 2001; Zaw et al., 2007; Zhang et al., 2014). However, these deposits display a set of characteristics that contrast with those of typical MVT-type deposits (Table 1; Huang et al., 2004, 2010; Zhou et al., 2013a, 2013b, 2013c, 2013d, 2013e, 2014a, 2014b), including ore-controlling thrust faults and fold structures (convergent ore-forming geodynamic setting), high grades ore of Pb + Zn (usually >10 wt.%), complex sources of ore-forming elements, moderate temperatures (150–280 °C), medium salinities (usually <15 wt.% NaCl), simple wall rock alterations and the lack of collapse breccias (e.g., Han et al., 2007a, 2007b; Zhou et al.,

Table 7
$^{87}Sr/^{86}Sr_{206\ Ma}$ values of basements, sedimentary rocks and basalts in the SYG province.

Whole-rock	Num.	$^{87}Sr/^{86}Sr_{206\ Ma}$		Source
		Range	Average	
Middle Permian Emeishan flood basalts	85	0.7039–0.7078	0.7058	Li and Qin (1988), Chen and Ran (1992), Deng et al. (2000), Shi et al. (2003), Huang et al. (2004), Jiang and Li (2005) and Zhou et al. (2013a, 2013b, 2014b)
Lower Permian Qixia Fm., Limestone	3	0.7073–0.7089	0.7075	
Upper Carboniferous Maping Fm., Limestone	2	0.7099–0.7100	0.7100	
Lower Carboniferous Baizuo Fm., Dolostone	5	0.7087–0.7101	0.7094	
Upper Devonian Zaige Fm., Limestone	2	0.7084–0.7088	0.7086	
Middle Devonian Qujing Fm., Dolostone	1	0.7101	0.7101	
Middle Devonian Haikou Fm., Sandstone	1	0.7111	0.7111	
Lower Cambrian carbonates	16	0.7084–0.7099	0.7091	
Lower Cambrian black shale	2	0.7120–0.7136	0.7128	
Upper Sinian Dengying Fm., Dolostone	2	0.7083–0.7096	0.7089	
Proterozoic folded basement rocks	5	0.7243–0.7288	0.7268	
Upper mantle		0.704 ± 0.002	0.704	Faure (1977)

$(^{87}Sr/^{86}Sr)_t = (^{87}Sr/^{86}Sr)_p - ^{87}Rb/^{86}Sr\ (e^{\lambda t} - 1)$, $\lambda_{Rb} = 1.41 \times 10^{-11}\ t^{-1}$, t = 206 Ma. Fm. = Formation.

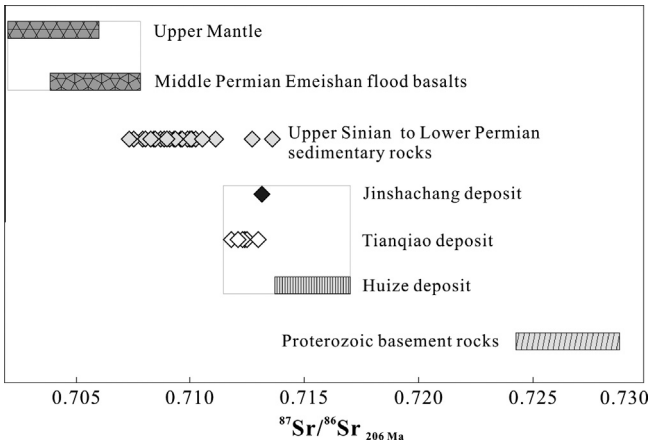

Fig. 9. Comparisons of $^{87}Sr/^{86}Sr_{206\ Ma}$ ratios among the Jinshachang, Tianqiao and Huize Pb–Zn deposits, Proterozoic basement rocks, Upper Sinian to Lower Permian sedimentary rocks, Middle Permian Emeishan flood basalts, and Upper Mantle (Faure, 1977). Data from the Huize and Tianqiao deposits, and whole-rock Sr isotopes are from previous studies, including Li and Qin (1988), Chen and Ran (1992), Deng et al. (2000), Shi et al. (2003), Huang et al. (2004), Jiang and Li (2005), Yin et al. (2009) and Zhou et al. (2013a, 2013b).

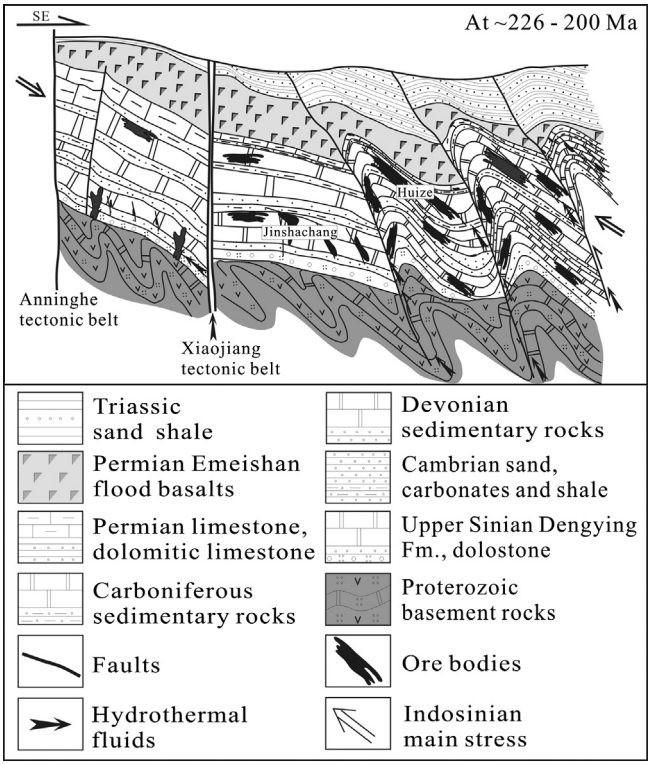

Fig. 10. Metallogenic model of the SYG Pb–Zn deposits (modified from Han et al., 2012). At ~226–200 Ma, the closure of the Palaeo-Tethys Ocean resulted in deformation of the strata through thrust fault-fold structures, which is known as the Indosinian Orogeny. Thermal activity related to this event resulted in circulation of hydrothermal fluids within basement and country rocks where they picked up metals and formed reduced sulfur, and then subsequent precipitation of these elements in favorable structural and lithological units.

2013a, 2013b, 2014a, 2014b). Although there is no direct genetic relationship between the basalts and Pb–Zn deposits, the basalts could have provided some metals to the hydrothermal system (e.g., Huang et al., 2004, 2010; Xu et al., 2014; Zhou et al., 2014a, 2014b; Zhang et al., 2014). Therefore, an alternative model (Fig. 10) is that the Jinshachang deposit is a carbonate-hosted, strata-bound, thrust fold-controlled, epigenetic deposit with fluids and metals derived from the Cambrian sedimentary strata. The mineralization process is similar to that of MVT-type deposits elsewhere, including extraction of ore-forming elements from Cambrian sedimentary rocks by convective circulation of hydrothermal fluids and subsequent precipitation of these elements in favorable structural and lithological units (Fig. 10; Hu and Zhou, 2012).

6. Conclusions

(1) H–O–S–Pb–Sr isotopes suggest that the Cambrian sedimentary rocks, in particular the black shale, are the most important fluid and metal sources for the Jinshachang deposit.

(2) Sphalerite yields an Rb–Sr isotopic age of 206.8 ± 3.7 Ma. This may represent the timing of Pb–Zn mineralization within the SYG province and suggests that the Jinshachang deposit formed during the Late Triassic related to late Indosinian Orogeny in response to the closure of the Paleo-Tethys Ocean.

(3) The Jinshachang deposit belongs to an epigenetic, carbonate-hosted, strata-bound and thrust fold-controlled deposit that is different from typical MVT deposits.

Acknowledgements

The research is jointly supported by the National Basic Research Program of China (No. 2014CB440905), the State Key Program of National Natural Science Foundation of China (No. 41430315), and the National Natural Science Foundation of China (Nos. 41102055 and 41272111). Thanks are given to Dr. Ping-Ping Liu and Prof. Mei-Fu Zhou for useful discussion and modification. Comments and suggestions from Prof. Bor-ming Jahn (Editor-in-Chief), Miss Irene Yao, and two anonymous reviewers greatly improved the quality of the paper.

References

Bai, J.H., Huang, Z.L., Zhu, D., Yan, Z.F., Zhou, J.X., 2013. Isotopic compositions of sulfur in the Jinshachang lead–zinc deposit, Yunnan, China. Acta Geol. Sin. (Engl. Ed.) 87, 1355–1369.

Basuki, N.I., Taylor, B.E., Spooner, E.T.C., 2008. Sulfur isotope evidence for thermochemical reduction of dissolved sulfate in Mississippi valley type zinc–lead mineralization, Bongara area, northern Peru. Econ. Geol. 103, 183–799.

Belshaw, N.S., Freedman, P.A., O'Nions, R.K., Frank, M., Guo, Y., 1998. A new variable dispersion double-focusing plasma mass spectrometer with performance illustrated for Pb isotopes. Int. J. Mass Spectrom. 181, 51–58.

Brannon, J.C., Podosek, F.A., McLimans, R.K., 1992. Alleghenian age of the Upper Mississippi Valley zinc–lead deposit determined by Rb–Sr dating of sphalerite. Nature 356, 509–511.

Carr, G.R., Dean, J.A., Suppel, D.W., Heithersay, P.S., 1995. Precise lead isotope fingerprinting of hydrothermal activity associated with Ordovician to Carboniferous metallogenic events in the Lachlan fold belt of New South Wales. Econ. Geol. 90, 1467–1505.

Chaussidon, M., Albarède, F., Sheppard, S.M.F., 1989. Sulphur isotope variations in the mantle from ion microprobe analyses of micro-sulphide inclusions. Earth Planet. Sci. Lett. 92, 144–156.

Chen, H.S., Ran, C.Y., 1992. Isotope Geochemistry of Copper Deposit in Kangdian Area. Geological Publishing House, Beijing, pp. 1–25 (in Chinese).

Christensen, J.N., Halliday, A.N., 1995. Direct dating of sulfides by Rb–Sr: a critical test using the Polaris Mississippi Valley-type Zn–Pb deposit. Geochim. Cosmochim. Acta 59, 5191–5197.

Christensen, J.N., Halliday, A.N., Vearncombe, J.R., Kesler, S.E., 1995. Testing models of large-scale crustal fluid flow using direct dating of sulfides: Rb–Sr evidence for early dewatering and formation of Mississippi Valley-type deposits, Canning Basin, Australia. Econ. Geol. 90, 877–884.

Claypool, G.E., Holser, W.T., Kaplan, I.R., Sakai, H., Zak, I., 1980. The age curves of sulfur and oxygen isotopes in marine sulfate and their mutual interpretation. Chem. Geol. 28, 199–260.

Clayton, R.N., Mayeda, T.K., 1963. The use of bromine pentafluoride in the extraction of oxygen from oxides and silicates for isotopic analysis. Geochim. Cosmochim. Acta 27, 43–52.

Clayton, R.N., O'Neil, J.R., Mayeda, T.K., 1972. Oxygen isotope exchange between quartz and water. J. Chem. Phys. 77, 3057–3067.

Cromie, P.W., Gosse, R.R., Zhang, P., Zhu, X., 1996. Exploration for carbonate-hosted Pb–Zn deposits, Sichuan, P.R.C. [abs.]: International Geological Congress, 30th, Beijing, China, p. 412 (Abstracts).

Deng, H.L., Li, C.Y., Tu, G.Z., Zhou, Y.M., Wang, C.W., 2000. Strontium isotope geochemistry of the Lemachang independent silver ore deposit, northeastern Yunnan, China. Sci. China (Ser. D): Earth Sci. 43, 337–346.

Dou, S., Liu, J.S., Zhou, J.X., 2014. Strontium isotopic geochemistry of Tianqiao Pb–Zn deposit, southwest China. Chin. J. Geochem. 33, 131–137.

Faure, G., 1977. Principles of Isotope Geology. John Wiley & Sons, New York, pp. 28–110.

Fontbote, L., Gorzawski, H., 1990. Genesis of the Mississippi Valley-type Zn–Pb deposit of San Vicente, central Peru: geologic and isotopic (Sr, O, C, S, Pb) evidence. Econ. Geol. 85, 1402–1437.

Gromek, P., Gleeson, S.A., Simonetti, A., 2012. A basement-interacted fluid in the N81 deposit, Pine Point Pb–Zn district, Canada: Sr isotopic analyses of single dolomite crystals. Miner. Deposita 47, 749–754.

Haest, M., Schneider, J., Cloquet, C., Latruwe, K., Vanhaecke, F., Muchez, P., 2010. Pb isotopic constraints on the formation of the Dikulushi Cu–Pb–Zn–Ag mineralisation, Kundelungu Plateau (Democratic Republic of Congo). Miner. Deposita 45, 393–410.

Han, R.S., Hu, Y.Z., Wang, X.K., Hou, B.H., Huang, Z.L., Chen, J., Wang, F., Wu, P., Li, B., Wang, H.J., Dong, Y., Lei, L., 2012. Mineralization model of rich Ge-Ag-bearing Zn-Pb polymetallic deposit concentrated district in northeastern Yunnan. China. Acta Geol. Sin. 86, 280–294 (in Chinese with English abstract).

Han, R.S., Liu, C.Q., Huang, Z.L., Chen, J., Ma, D.Y., Lei, L., Ma, G.S., 2007a. Geological features and origin of the Huize carbonate-hosted Zn–Pb–(Ag) District, Yunnan, South China. Ore Geol. Rev. 31, 360–383.

Han, R.S., Zou, H.J., Hu, B., Hu, Y.Z., Xue, C.D., 2007b. Features of fluid inclusions and sources of ore-forming fluid in the Maoping carbonate-hosted Zn–Pb–(Ag–Ge) deposit, Yunnan, China. Acta Petrol. Sin. 23, 2109–2118.

Heijlen, W., Muchez, P., Banks, D.A., Schneider, J., Kucha, H., Keppens, E., 2003. Carbonate-hosted Zn–Pb deposits in Upper Silesia, Poland: origin and evolution of mineralizing fluids and constraints on genetic models. Econ. Geol. 98, 911–932.

Hu, R.Z., Zhou, M.F., 2012. Multiple Mesozoic mineralization events in South China – an introduction to the thematic issue. Miner. Deposita 47, 579–588.

Huang, Z.L., Li, W.B., Chen, J., Han, R.S., Liu, C.Q., Xu, C., Guan, T., 2003. Carbon and oxygen isotope constraints on the mantle fluids join the mineralization of the Huize super-large Pb–Zn deposits, Yunnan Province, China. J. Geochem. Explor. 78 (79), 637–642.

Huang, Z.L., Chen, J., Han, R.S., Li, W.B., Liu, C.Q., Zhang, Z.L., Ma, D.Y., Gao, D.R., Yang, H.L., 2004. Geochemistry and Ore-formation of the Huize Giant Lead–Zinc Deposit, Yunnan, province, China: Discussion on the Relationship between the Emeishan Flood Basalts and Lead–Zinc Mineralization. Geological Publishing House, Beijing, pp. 1–214 (in Chinese).

Huang, Z.L., Li, X.B., Zhou, M.F., Li, W.B., Jin, Z.G., 2010. REE and C–O isotopic geochemistry of calcites from the word-class Huize Pb–Zn deposits, Yunnan, China: implication for the ore genesis. Acta Geol. Sin. (Engl. Ed.) 84, 597–613.

Jiang, Y.H., Li, S.R., 2005. Study on the isotope data tracing and isotopic chronology in the black-rock series type Ni–Mo deposit in the Lower Cambrian in Hunan and Guizhou provinces. J. Mineral. Petrol. 25, 62–66 (in Chinese with English abstract).

Leach, D.L., Sangster, D., Kelley, K.D., Large, R.R., Garven, G., Allen, C., Gutzmer, J., Walters, S., 2005. Sediment-hosted lead–zinc deposits: a global perspective. Economic Geology 100th Anniversary, pp. 561–607.

Leach, D.L., Bradley, D.C., Huston, D., Pisarevsky, S.A., Taylor, R.D., Gardoll, S.J., 2010. Sediment-hosted lead–zinc deposits in Earth history. Econ. Geol. 105, 593–625.

Li, F.H., Qin, J.M., 1988. Presinian System in Kangdian Area. Chongqing Press, Chongqing, pp. 15–45 (in Chinese).

Li, Q.L., Chen, F.K., Wang, X.L., Li, C.F., 2005. Ultra-low procedural blank and the single grain mica Rb–Sr isochron dating. Chin. Sci. Bull. 50, 2861–2865.

Li, W.B., Huang, Z.L., Yin, M.D., 2007. Dating of the giant Huize Zn–Pb ore field of Yunnan province, southwest China: constrains from the Sm–Nd system in hydrothermal calcite. Resour. Geol. 57, 90–97.

Li, Q.L., Chen, F.K., Yang, J.H., Fan, H.R., 2008. Single grain pyrite Rb–Sr dating of the Linglong gold deposit, eastern China. Ore Geol. Rev. 34, 263–270.

Lin, Z.Y., Wang, D.H., Zhang, C.Q., 2010. Rb–Sr isotopic age of sphalerite from the Paoma lead–zinc deposit in Sichuan Province and its implications. Geol. China 37, 488–494 (in Chinese with English abstract).

Liu, W.Z., 1989. Geological characteristics and genesis of the Jinshachang lead–zinc deposit in Yunnan Province, China. J. Chengdu College Geol. 16, 11–19 (in Chinese with English abstract).

Liu, H.C., Lin, W.D., 1999. Study on the Law of Pb–Zn–Ag Ore Deposit in Northeast Yunnan, China. Yunnan University Press, Kunming, pp. 1–468 (in Chinese).

Mao, J.W., Zhou, Z.H., Feng, C.Y., Wang, Y.T., Zhang, C.Q., Peng, H.J., Miao, Y., 2012. A preliminary study of the Triassic large-scale mineralization in China and its geodynamic setting. Geol. China 39, 1437–1471 (in Chinese with English abstract).

Mirnejad, H., Simonetti, A., Molasalehi, F., 2011. Pb isotopic compositions of some Zn–Pb deposits and occurrences from Urumieh-Dokhtar and Sanandaj-Sirjan Zones in Iran. Ore Geol. Rev. 39, 181–187.

Muchez, P., Heijlen, W., Banks, D., Blundell, D., Boni, M., Grandia, F., 2005. Extensional tectonics and the timing and formation of basin-hosted deposits in Europe. Ore Geol. Rev. 27, 241–267.

Nakai, S., Halliday, A.N., Kesler, S.E., Jones, H.D., Kyle, J.R., Lanes, T.E., 1993. Rb–Sr dating of sphalerite from Mississippi Valley-type (MVT) ore deposits. Geochim. Cosmochim. Acta 57, 417–427.

Pirajno, F., 2013. The Geology and Tectonic Setting of China's Mineral Deposits. Springer, Berlin, pp. 123–183.

Qiu, Y.M., Gao, S., McNaughton, N.J., Groves, D.I., Ling, W.L., 2000. First evidence of >3.2 Ga continental crust in the Yangtze craton of south China and its implications for Archean crustal evolution and Phanerozoic tectonics. Geology 28, 11–14.

Reid, A., Wilson, C.J.L., Shun, L., Pearson, N., Belousova, E., 2007. Mesozoic plutons of the Yidun Arc, SW China: U/Pb geochronology and Hf isotopic signature. Ore Geol. Rev. 31, 88–106.

Seal, I.R., 2006. Sulfur isotope geochemistry of sulfide minerals. Rev. Mineral. Geochem. 61, 633–677.

Shi, H., Huang, S.J., Shen, L.C., Zhang, M., 2003. Strontium isotope composition of the Cambrian Luojiaguo section in Xiushan, Chongqing and its stratigraphic significance. J. Stratigraphy 27, 71–76 (in Chinese with English abstract).

Sun, W.H., Zhou, M.F., Gao, J.F., Yang, Y.H., Zhao, X.F., Zhao, J.H., 2009. Detrital zircon U–Pb geochronological and Lu–Hf isotopic constraints on the Precambrian magmatic and crustal evolution of the western Yangtze Block, SW China. Precambr. Res. 172, 99–126.

Wang, R., Zhang, C.Q., Wu, Y., Wei, C., 2012. The age of diabase in Tianbaoshan Pb–Zn deposit and the genetic relationship between lead–zinc mineralization and the diabase. Miner. Deposits 31, 449–450 (in Chinese).

Wang, W., Zhou, M.F., Zhao, X.F., Chen, W.T., Yan, D.P., 2014. Late Paleoproterozoic to Mesoproterozoic rift successions in SW China: Implication for the Yangtze Block-North Australia–Northwest Laurentia connection in the Columbia supercontinent. Sed. Geol. 309, 33–47.

Wu, Y., 2013. The Age and Ore-forming Process of MVT Deposits in the Boundary Area of Sichuan–Yunnan–Guizhou Provinces, Southwest China. A Dissertation Submitted to China University of Geosciences for Doctoral Degree, Beijing, pp. 20–171 (in Chinese with English abstract).

Wu, Y., Zhang, C.Q., Mao, J.W., Ouyang, H.G., Sun, J., 2013. The genetic relationship between hydrocarbon systems and Mississippi Valley-type Zn–Pb deposits along the SW margin of Sichuan Basin, China. Int. Geol. Rev. 55, 941–957.

Xie, J.R., 1963. Introduction of the Chinese Ore Deposits. Scientific Books Publishing House, Beijing, pp. 1–71 (in Chinese).

Xu, Y.K., Huang, Z.L., Zhu, D., Luo, T.Y., 2014. Origin of hydrothermal deposits related to the Emeishan magmatism. Ore Geol. Rev. 63, 1–8.

Yan, D.P., Zhou, M.F., Song, H.L., Wang, X.W., Malpas, J., 2003. Origin and tectonic significance of a Mesozoic multi-layer over-thrust system within the Yangtze Block (South China). Tectonophysics 361, 239–254.

Ye, L., Cook, N.J., Ciobanu, C.L., Liu, Y.P., Zhang, Q., Liu, T.G., Gao, W., Yang, Y.L., Danyushevsky, L., 2011. Trace and minor elements in sphalerite from base metal deposits in South China: a LA-ICPMS study. Ore Geol. Rev. 39, 188–217.

Yin, M.D., Huang, Z.L., Li, W.B., 2009. Rb–Sr isotopic dating of sphalerite from the giant Huize Pb–Zn ore field, Yunnan province, southwestern China. Chin. J. Geochem. 28, 70–75.

Zartman, R.E., Doe, B.R., 1981. Plumbotectonics – the model. Tectonophysics 75, 135–162.

Zaw, K., Peters, S.G., Cromie, P., Burrett, C., Hou, Z., 2007. Nature, diversity of deposit types and metallogenic relations of South China. Ore Geol. Rev. 31, 3–47.

Zhang, C.Q., Wu, Y., Hou, L., Mao, J.W., 2014. Geodynamic setting of mineralization of Mississippi Valley-type deposits in world-class Sichuan–Yunnan–Guizhou Zn–Pb triangle, southwest China: implications from age-dating studies in the past decade and the Sm–Nd age of the Jinshachang deposit. J. Asian Earth Sci. http://dx.doi.org/10.1016/j.jseaes.2014.08.013.

Zhao, X.F., Zhou, M.F., Li, J.W., Sun, M., Gao, J.F., Sun, W.H., Yang, J.H., 2010. Late Paleoproterozoic to early Mesoproterozoic Dongchuan group in Yunnan, SW China: implications for tectonic evolution of the Yangtze Block. Precambr. Res. 182, 57–69.

Zheng, Y.F., Chen, J.F., 2000. Stable Isotope Geochemistry. Science Press, Beijing, pp. 10–50 (in Chinese).

Zheng, M.H., Wang, X.C., 1991. Genesis of the Daliangzi Pb–Zn deposit in Sichuan, China. Econ. Geol. 86, 831–846.

Zhou, C.X., Wei, C.S., Guo, J.Y., 2001. The source of metals in the Qilingchang Pb–Zn deposit, Northeastern Yunnan, China: Pb–Sr isotope constraints. Econ. Geol. 96, 583–598.

Zhou, M.F., Yan, D.P., Kennedy, A.K., Li, Y.Q., Ding, J., 2002a. SHRIMP zircon geochronological and geochemical evidence for Neo-proterozoic arc-related magmatism along the western margin of the Yangtze Block, South China. Earth Planet. Sci. Lett. 196, 1–67.

Zhou, M.F., Malpas, J., Song, X.Y., Kennedy, A.K., Robinson, P.T., Sun, M., Lesher, M., Keays, R.R., 2002b. A temporal link between the Emeishan large igneous province (SW China) and the end-Guadalupian mass extinction. Earth Planet. Sci. Lett. 196, 113–122.

Zhou, J.X., Huang, Z.L., Zhou, G.F., Li, X.B., Ding, W., Bao, G.P., 2010. Sulfur isotopic compositions of the Tianqiao Pb–Zn ore deposit, Guizhou province, China: implications for the source of sulfur in the ore-forming fluids. Chin. J. Geochem. 29, 301–306.

Zhou, J.X., Huang, Z.L., Zhou, G.F., Li, X.B., Ding, W., Bao, G.P., 2011. Trace elements and rare earth elements of sulfide minerals in the Tianqiao Pb–Zn Ore deposit, Guizhou Province, China. Acta Geol. Sin. (Engl. Ed.) 85, 189–199.

Zhou, J.X., Huang, Z.L., Zhou, M.F., Li, X.B., Jin, Z.G., 2013a. Constraints of C–O–S–Pb isotope compositions and Rb–Sr isotopic age on the origin of the Tianqiao carbonate-hosted Pb–Zn deposit, SW China. Ore Geol. Rev. 53, 77–92.

Zhou, J.X., Huang, Z.L., Bao, G.P., 2013b. Geological and sulfur–lead–strontium isotopic studies of the Shaojiwan Pb–Zn deposit, southwest China: implications for the origin of hydrothermal fluids. J. Geochem. Explor. 128, 51–61.

Zhou, J.X., Gao, J.G., Chen, D., Liu, X.K., 2013c. Ore genesis of the Tianbaoshan carbonate-hosted Pb–Zn deposit, Southwest China: geologic and isotopic (C–H–O–S–Pb) evidence. Int. Geol. Rev. 55, 1300–1310.

Zhou, J.X., Huang, Z.L., Yan, Z.F., 2013d. The origin of the Maozu carbonate-hosted Pb–Zn deposit, southwest China: constrained by C–O–S–Pb isotopic compositions and Sm–Nd isotopic age. J. Asian Earth Sci. 73, 39–47.

Zhou, J.X., Huang, Z.L., Gao, J.G., Yan, Z.F., 2013e. Geological and C–O–S–Pb–Sr isotopic constraints on the origin of the Qingshan carbonate-hosted Pb–Zn deposit, SW China. Int. Geol. Rev. 55, 904–916.

Zhou, J.X., Huang, Z.L., Zhou, M.F., Zhu, X.K., Muchez, P., 2014a. Zinc, sulfur and lead isotopic variations in carbonate-hosted Pb–Zn sulfide deposits, southwest China. Ore Geol. Rev. 58, 41–54.

Zhou, J.X., Huang, Z.L., Lv, Z.C., Zhu, X.K., Gao, J.G., Mirnejad, H., 2014b. Geology, isotope geochemistry and ore genesis of the Shanshulin carbonate-hosted Pb–Zn deposit, southwest China. Ore Geol. Rev. 63, 209–225.